Population Balance PSD Model for Emulsion Polymerization with Steric Stabilizers

Charles D. Immanuel and Francis J. Doyle III
Dept. of Chemical Engineering, University of Delaware, Newark, DE 19716

Cajetan F. Cordeiro and Sekhar S. Sundaram
Air Products and Chemicals Inc., Allentown, PA 18195

A detailed population balance model is developed for the particle-size distribution (PSD) in the emulsion copolymerization of vinyl acetate and butyl acrylate, with nonionic poly(ethylene oxide) surfactants and a redox initiator pair (t-butyl hydrogen peroxide and sodium formaldehyde sulphoxylate). The model accounts for the effects of the nucleation, growth, and coagulation events on the evolution of the PSD. The study addresses the modeling of the coagulation kernel (time-varying and size-dependent intrinsic coagulation rate) under nonionic surfactants. The coagulation-inclusive model results show significant differences from the results generated by a coagulation-free model (even under low solids conditions). More importantly, the coagulation-inclusive model predicts to a reasonable accuracy the experimental data on the full PSD.

Introduction

In emulsion polymerization, the main locus of polymerization lies within organic particles (in the size range of about 2 nm to 1 μ), which are dispersed in the aqueous phase. The particle-size distribution (PSD) is one of the most important characteristics of the emulsion as it determines most critical properties, including the rheological properties, adhesion, drying characteristics, solids content, film-forming properties, optical properties, and so on. Thus, the control of PSD is well-motivated, which requires a detailed model describing the evolution of the PSD, accounting for the complex mechanisms. The polymerization is primarily initiated in the aqueous phase, and results in aqueous-phase oligomers. However, both the monomers and polymers have a limited solubility in the aqueous phase, thereby limiting the extent of polymerization in this continuous phase. The particle phase results by two major mechanisms. The primary mechanism of particle formation is micellar nucleation, which is effected by the entry of an oligomer from the aqueous phase into a micellar aggregate of amphiphilic surfactants. These micelles are formed under a high concentration of surfactant molecules in the aqueous phase, exceeding the critical micelle concentration (cmc) threshold. The second mechanism of particle formation does not explicitly involve the heterogenous surfactant molecules, and is termed homogenous nucleation. This occurs by the precipitation of the aqueous-phase oligomers upon attainment of the critical chain length. The nucleated particles participate in two major processes. One is the growth in size due to the polymerization of the radicals within them. The second is the coagulation with each other, due to colloidal instability. Thus, the PSD is determined by the interplay of three major processes—nucleation, growth, and coagulation. There is considerable literature on the modeling of the full PSD in a population-balance framework: Min and Ray (1974); Rawlings and Ray (1988a,b); Chen and Wu (1988); Saldivar et al. (1998); Coen et al. (1998); Crowley et al. (2000); Araujo et al. (2001); Meadows et al. (2002). These comprise two schools of models: one based on assumptions in terms of the average number of radicals/particle, and the other more general. See Immanuel et al. (2002a) for a more detailed review on the modeling of PSD in emulsion polymerization.

The mechanism of particle stabilization, and, hence, the modeling of the coagulation phenomenon, is primarily dependent upon the type of the surfactant used. While the ionic surfactants stabilize the particles by electrostatic repulsion, the nonionic surfactants cause the stabilization due to many different, relatively less understood, mechanisms, the major

Correspondence concerning this article should be addressed to F. J. Doyle III at this current address: University of California, Santa Barbara, Chemical Engineering Dept., Santa Barbara, CA 93106.

one being steric stabilization (Napper, 1983; Gilmore et al., 1993). The coagulation kernel (intrinsic coagulation rate) is modeled in terms of an activation barrier and frequency factor (Arrhenius form), utilizing colloidal theory and the forces and potentials between the particles to calculate these terms. This approach results in intrinsic coagulation rates that are not only size-dependent, but also vary along the batch depending upon the conditions of the latex. Thus, a substantial computational load is involved in the calculation of the coagulation kernels. Most of the studies reported on coagulation modeling have considered ionic surfactants (Richards et al., 1989; Coen et al., 1998; Melis et al., 2000), with the coagulation constants being calculated by employing the well-known DLVO theory (Israelachvili, 1998). The modeling of the coagulation kernel under nonionic stabilization is not as well documented as its ionic counterpart. One significant study that addresses the effect of steric forces for PVC bulk or suspension polymerization is presented by Kiparissides et al. (1993), in which the steric potential due to nonionic surfactants is modeled using the Hesselink-Vrij-Overbeek (HVO) theory, based on entropic considerations. Some recent studies (Fritz et al., 2002) have modeled the forces due to combined electrostatic and steric repulsion, characterizing the steric repulsion in terms of the osmotic pressure and the entropic effects. Another aspect that is important from the perspective of coagulation is the effect of the agitation in the reactor. In general, the effect of mixing on coagulation could be correlated with the shear stress imparted on the particles, with the shear effects enhancing the coagulation rates over those that would prevail under shear-free conditions.

The current study utilizes nonionic poly(ethylene oxide)-based surfactants. A comprehensive population balance model has been developed for the evolution of PSD in the semi-batch emulsion polymerization of vinyl acetate (VAc) and butyl acrylate (BuA), accounting for the nucleation and growth effects (assuming that the coagulation events are unimportant in the low solids content regime that was considered in the study) (Immanuel et al., 2002a). As a significant departure from earlier models, which either employed an algebraic empirical expression to model the average number of radicals/particle or made some restrictive assumptions about the number of radicals inside the particles, an equation derived from first principles was employed to model this quantity, incorporating its size-dependence. This approach captures the broadening of the distribution seen in the experimental data well, justifying the increased computational load. Another novelty in the model is the incorporation of the partitioning of the surfactants into the dispersed phases, a phenomenon unique to nonionic surfactants (Piirma and Chang, 1982; Ozdeger et al., 1997). This modification captures the complexity in the nucleation pattern and the evolution of the PSD in using nonionic surfactants. The experimental implementation of the optimal recipes developed using the above model reveals the presence of coagulation events even under these low-solids conditions (Immanuel and Doyle III, 2002c), in some cases strong enough to cause an irreversible modification to the distribution. This clearly highlights the importance of incorporating the coagulation events into the model, which is the topic of this article. In calculating the coagulation kernel, steric hindrance is assumed to be the predominant mechanism of stabilization. However, allowances are made to account for other mechanisms, such as the shear effects. The model predictions provide a substantially-better match to the experimental data after the incorporation of these coagulation effects.

Model Formulation

The population balance equation describing the evolution of the PSD in emulsion polymerization is given by

$$\frac{\partial}{\partial t}F(r,t)+\frac{\partial}{\partial r}\left[F(r,t)\,\Re_{\text{growth}}(r,t)\right]=\Re_{\text{nuc}}(r,t)+\Re_{\text{coag}}(r,t) \quad (1)$$

where $F(r,t)$ is the particle density function, defined such that $F(r,t)dr$ is the moles of particles of size between r and $r+dr$. The terms $\Re_{\text{nuc}}(r,t)$, $\Re_{\text{growth}}(r,t)$ and $\Re_{\text{coag}}(r,t)$ account for the nucleation, growth, and coagulation events, respectively. Nucleation is usually restricted to the lower boundary condition, thereby reducing the population balance equation to

$$\frac{\partial}{\partial t}F(r,t)+\frac{\partial}{\partial r}\left[F(r,t)\,\Re_{\text{growth}}(r,t)\right]=\Re_{\text{coag}}(r,t) \quad (2)$$

A pseudo-steady state is assumed in specifying the boundary condition (a common practice when the growth rate is nonzero (Saldivar et al., 1998). Thus, the boundary condition becomes $F(r_{\text{nuc}},t)\,\Re_{\text{growth}}(r_{\text{nuc}},t)=\Re_{\text{nuc}}(t)$. The solution of the population balance equation (Eq. 2) (which is an integro-hyperbolic partial differential equation), along with the other relevant equations, is a challenging and computationally-intensive task. In the earlier study (Immanuel et al., 2002a), the technique of Orthogonal Collocation on Finite Elements (OCFE) was used to discretize the partial differential equation into a system of differential algebraic equations (DAEs), and the resultant combined system of DAEs was solved using the FORTRAN-based DAE solver DDASSL. The details in modeling the nucleation and growth terms ($\Re_{\text{nuc}}(t)$ and $\Re_{\text{growth}}(r,t)$) along with the detailed kinetic scheme for the process can be found in Immanuel et al. (2002a). The calculations involve partitioning considerations for the surfactants and monomers, and material balances for the aqueous phase oligomers and the particle phase polymers. The calculation of the coagulation term is detailed here.

Coagulation modeling

The coagulation rate $\Re_{\text{coag}}(r,t)$ involves two terms, one accounting for the formation of a particle by coagulation of particles of smaller sizes, and the other accounting for the depletion of a particle by coagulation with other particles. Thus, $\Re_{\text{coag}}(r,t)=\Re_{\text{formation}}(r,t)-\Re_{\text{depletion}}(r,t)$. The formation term $\Re_{\text{formation}}(r,t)$ (in moles/m-s) is modeled as

$$\Re_{\text{formation}}(r,t)=\frac{1}{V_w}\int_{r'=r_{\text{nuc}}}^{r/2^{1/3}}\beta(r',r'')F(r',t)F(r'',t)dr'\frac{dr''}{dr} \quad (3)$$

In the above equation, r' and r'' denote the sizes of two (smaller) particles that form a particle of size r upon coagulation. These are related by a volume additivity condition as $(r')^3 + (r'')^3 = r^3$. Thus, the terms dr''/dr in Eq. 3, which represents the differential of the size of the second particle (involved in coagulation with the first particle of fixed state r') to the differential of the size of the particle formed, is given by

$$\frac{dr''}{dr} = \frac{r^2}{\left(r^3 - (r')^3\right)^{2/3}} \tag{4}$$

Thus, the formation term becomes

$$\mathfrak{R}_{\text{formation}}(r,t) = \frac{1}{V_w}\int_{r'=r_{\text{nuc}}}^{r/2^{1/3}} \beta(r',r'')F(r',t)F(r'',t)\frac{r^2}{\left(r^3-(r')^3\right)^{2/3}}dr' \tag{5}$$

The upper limit of integration $r/2^{1/3}$ is to avoid double counting the coagulation events, and corresponds to the case in which the two coagulating particles are of the same size. The depletion term is given by

$$\mathfrak{R}_{\text{depletion}}(r,t) = \frac{1}{V_w}\int_{r_{\text{nuc}}}^{r_{\max}} \beta(r,r')F(r,t)F(r',t)dr' \tag{6}$$

where $r_{\max}$ is the size of the largest particle that can participate in coagulation.

The calculation of the intrinsic coagulation rate (coagulation kernel) β involves considerations of the forces and potentials between the particles. In the current study with nonionic surfactants, the stabilizing mechanism is assumed to be steric hindrance, which is caused by the bulkiness of the surfactant chains that prevents the particles onto which the chains are adsorbed from approaching each other. As stated previously, there are few studies addressing the modeling of the steric potential, particularly in the context of population balance models in emulsion polymerization. It is essential to develop a model that can predict the experimental results well, while simultaneously being of a low computational complexity. Thus, in this study, simple expressions for the steric potential (analogous to those commonly employed for electrostatic and van der Waals' potentials) are used. The steric repulsive potential between two flat objects due to the surfactant chains adsorbed onto their surfaces is given by Israelachvili (1998) (p. 295)

$$\psi_R^f(D) = \frac{100L}{\pi}\Gamma^{3/2}kTe^{-\pi D/L} \tag{7}$$

where D is the separation distance between the objects. The above equation is valid for separation distances up to twice the extensional length (L) of the surfactant chain into the aqueous phase, which is given by $L = \Gamma^{1/2}R_F^{5/3}$. Γ is the surface coverage of the particles with surfactants (based on the partitioning calculation of the surfactants among the various phases) modeled as

$$\Gamma = \frac{\Gamma_\infty K_{\text{ad}} S_w N_A}{1 + K_{\text{ad}} S_w} \tag{8}$$

In the above equation, K_{ad} is the adsorption equilibrium constant for the surfactants and Γ_∞ is the equilibrium surface coverage (Langmuir constants), with N_A being the Avogadro number. R_F is the Flory radius, which is related to the radius of gyration of the polymeric surfactant chain (R_g) as $R_F = \alpha R_g$. Here, α accounts for the interaction of the surfactant with the solver (water). The radius of gyration can be calculated as $R_g = l\sqrt{n}/\sqrt{6} = l\sqrt{M/M_0}/\sqrt{6}$, where l is the effective segment length (of the polymeric surfactant chain), n is the number of segments in the chain, M is the molecular weight of the surfactant chain, and M_0 is the molecular weight of a monomeric unit in the chain.

The Derjaguin approximation (Israelachvili, 1998) can be employed to extend Eq. 7 to obtain the repulsive potential between spherical particles. Thus, the repulsive force between two spherical particles of size r and r', separated by a distance D, is given by

$$F_R(D) = \frac{2\pi rr'}{r+r'}\frac{100L}{\pi}\Gamma^{3/2}kTe^{-\pi D/L} \tag{9}$$

This equation is again valid for $(r + r') < D < 2L$. Using the relation between force and potential, $F_R(D) = -(\partial\psi_R(D)/\partial D)$, one can obtain the steric potential as

$$\psi_R(D) = -\int F_R(D)d(D) = \frac{2rr'}{r+r'}\frac{100L^2}{\pi}\Gamma^{3/2}kTe^{-\pi D/L} + c \tag{10}$$

where c is a constant of integration. An adjustable constant is introduced into the above equation to account for the various mechanistic and parametric uncertainties in the model, thereby casting the repulsive potential as

$$\psi_R(D) = c_2\frac{2rr'}{r+r'}\frac{100L^2}{\pi}\Gamma^{3/2}kTe^{-\pi D/L} + c' \tag{11}$$

where c_2 is the adjustable constant, and $c' = c_2 c$.

The van der Waals' attractive potential is relatively well known, and is modeled as [for all $D > (r + r')$]

$$\psi_A(D) = \frac{A}{6}\left[\frac{2rr'}{D^2-(r+r')^2} + \frac{2rr'}{D^2-(r-r')^2} + \ln\left(\frac{D^2-(r+r')^2}{D^2-(r-r')^2}\right)\right] \tag{12}$$

In this equation, A is the Hamakar constant, which accounts for the effects of the various intrinsic (internal) interactions between the particles that result in the net attractive potential.

The net interaction potential, $\psi(D) = \psi_R(D) - \psi_A(D)$, can be utilized to calculate the intrinsic coagulation rate using established procedures (Melis et al., 2000), as follows: the

Fuch's stability ratio $W(r,r')$, which has a reciprocal relationship to the fraction of collision events that result in a successful coagulation event (activation barrier), is calculated as

$$W(r,r') = (r+r')\int_{D=(r+r')}^{\infty} \frac{\exp\left(\frac{\psi(D)}{kT}\right)}{D^2} d(D) \quad (13)$$

(k is the Boltzmann constant and T is the temperature of the emulsion). The stability ratio is related to the intrinsic coagulation rate using the first-order Smoluchowski equation as follows

$$\beta(r,r') = c_1 \frac{4\pi D_0 (r+r')}{W} \quad (14)$$

In Eq. 14, c_1 is another adjustable constant which subsumes the constant c' in Eq. 11, besides providing a way to account for the shear effects. This is based on the hypothesis that the shear effects enhance the coagulation rate over that under shear-free conditions (diffusion vs. convection analogy) (Evans and Wennerstrom, 1999). The diffusion coefficient D_0 is given by

$$D_0 = \frac{kT}{6\pi\mu}\left(\frac{1}{r}+\frac{1}{r'}\right) \quad (15)$$

Here, μ is the viscosity of the emulsion latex, related to the solids content as $\mu = \mu_0/[(1-(sc/sc_{\text{ref}}))]^2$, with μ_0 being the viscosity of water at the reaction temperature, sc, the latex solids content and sc_{ref}, a reference solids content.

Results and Discussion

Table 1 lists some of the model parameters adopted in this study on the copolymerization of vinyl acetate (VAc) and butyl acrylate (BuA) under a nonionic poly(ethylene oxide) surfactant, and a redox pair of t-butyl hydrogen peroxide (tBHP) and sodium formaldehyde sulphoxylate (SFS) for initiation. The other model parameters involved are available in Immanuel et al. (2002a). The straightforward solution methodology based on Orthogonal Collocation on Finite Elements results in a stiff system of equations, with condition numbers of the order of 10^4 in the regime of nucleation. This in turn results in large computation times. Incorporating the coagulation effects further increases the computational load, due to the intensive nature of the coagulation calculations. To circumvent this problem, an efficient computational technique, based on an order reduction effected by the decomposition of the fast and the slow kinetics, is employed (Immanuel and Doyle III, 2002b). The technique is based on a finite-element discretization of the domain of particle size. However, unlike one of the standard finite-element techniques, the particle count within each finite element ("bin") is updated employing a two-tier algorithm. In the first tier of the algorithm, the individual rates of nucleation, growth, and coagulation within each finite element are calculated (holding the PSD constant). In the second tier of the algorithm, the PSD is updated using the individual rates calculated in the first tier. Iteration over these two tiers is not essential due to the explicit formation adopted here. See Immanuel and Doyle III (2002b) for more details on the technique. For the present simulations, 250 finite elements with a uniform width of 2 nm radius are employed. Also, to reduce the computational load, the intrinsic coagulation rate $\beta(r,r')$ is updated only once every 10 min of batch time.

Table 1. Kinetic and Physical Constants

A	5.5×10^{-21} J
$k_{t11} = k_{t11}^{w}$	1.05×10^{7} L/mol·s
Γ_∞	7.5×10^{-6} mol/m^2
K_{ad}	4×10^{4} L/mol
cmc	2×10^{-5} mol/L
k_{r1}	0.1 L/mol·s
sc_{ref}	0.6
c_1	1×10^{-5}
c_2	1×10^{-10}
l	1 nm
M	616 g/mol
M_0	68.4 g/mol
$r_{\text{cut-off}}$	66 nm

Analysis of base case recipe

A typical simulation result is presented next with particular emphasis on the analysis of the coagulation kernel and its sensitivity to the process inputs. A comparison of the improvement obtained relative to the previous coagulation-free model predictions, and validation against experimental data, are presented in the next subsection. Figure 1 shows a plot of the van der Waals' attractive potential between particles of various sizes, separated by a representative distance of $D =$ 1.07 μm. Figure 2 shows similar plots of the repulsive potential between particles of various sizes, separated by the same distance of 1.07 μm. Figures 2a, 2b, and 2c correspond respectively to 30 min, 70 min, and 120 min of the recipe shown in Figure 3. In Figure 3, the monomer feeds (VAc and BuA) are pure components, while the feeds of the surfactant, tBHP and SFS are aqueous solutions with 22.7 wt. %, 3.33 wt. %, and 3.41 wt. % concentrations, respectively. The initial mix-

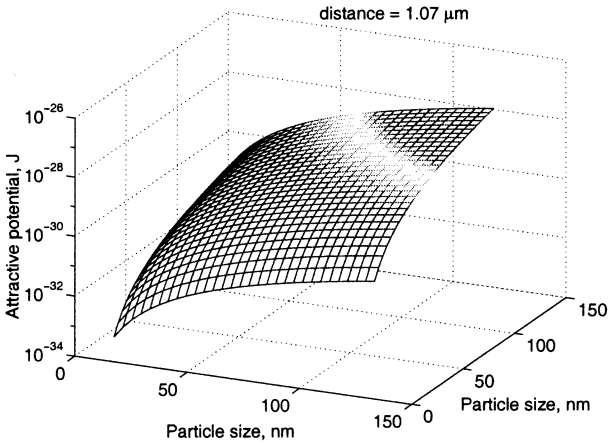

Figure 1. van der Waals' attractive potential between particles separated by a representative distance of $D = 1.07$ μm.

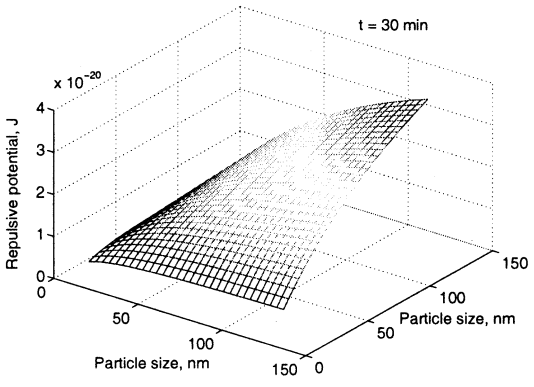

(a) $t = 30\ min,\ S_w = 0.9 \times 10^{-4}\ moles/liter$

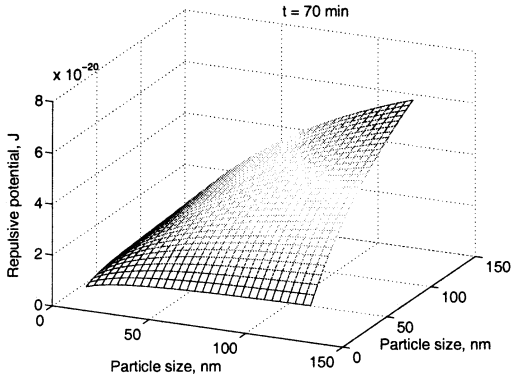

(b) $t = 70\ min,\ S_w = 3.8 \times 10^{-4}\ moles/liter$

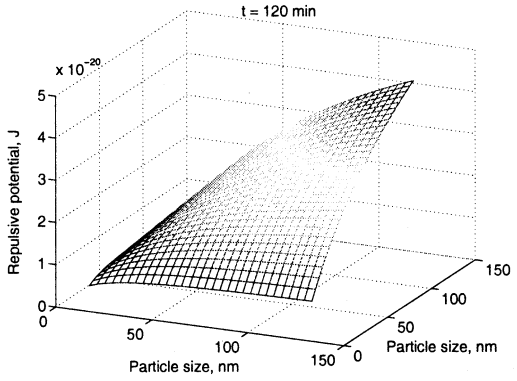

(c) $t = 120\ min,\ S_w = 1.2 \times 10^{-4}\ moles/liter$

Figure 2. Steric repulsive potential between particles separated by a distance of $D = 1.07\ \mu$m at different time instances, indicating the dependence on the free surfactant concentration S_w.

ture consists of 1 L DI water, 52 g VAc, 0.1 g ferrous ammonium sulfate as a coordination agent between tBHP and SFS, and a buffer for pH. As an attempt to draw a correlation between the coagulation kernel and the free surfactant concentration, Figure 4 shows the profile of the free surfactant concentration S_w over the course of the batch (top plot) and

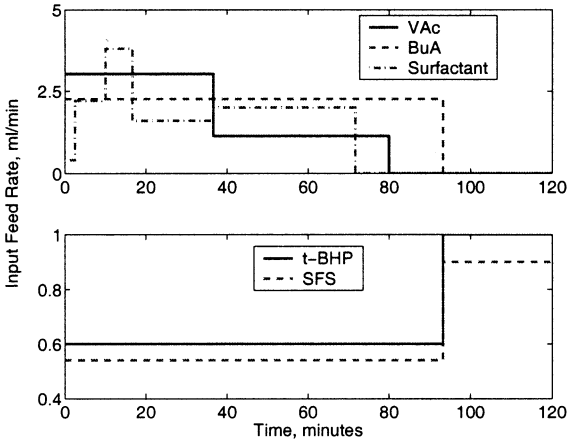

Figure 3. Nominal feed profile for semi-batch emulsion polymerization (base case).

the total swollen particle area (bottom plot). The plot shows that S_w varies profoundly during the batch. It increases from 10 min up to approximately 17 min, caused partly by the increase in the surfactant feed rate at this time (Figure 3), but also due to the depletion of the monomer droplets and the associated release of *absorbed* surfactants (figure not shown). Subsequently, it remains almost constant up to approximately 37.5 min, as the reduced feed rate of the surfactant solution at this time is just sufficient to compensate for the increase in the total surface area of the particles due to growth (Figure 4 —bottom plot). After 37.5 min, S_w begins to increase again due to the increased feed rate, up to approximately 70 min. Thereafter, S_w drops until approximately 95 min (due to adsorption onto the growing particles). Beyond 95 min, S_w remains almost constant as there is no further increase in the particle surface area. The repulsive potential (Figure 2) shows a considerable sensitivity to the free surfactant concentration S_w as expected (through the dependence on Γ). The high value of S_w at 70 min results in a higher repulsive potential

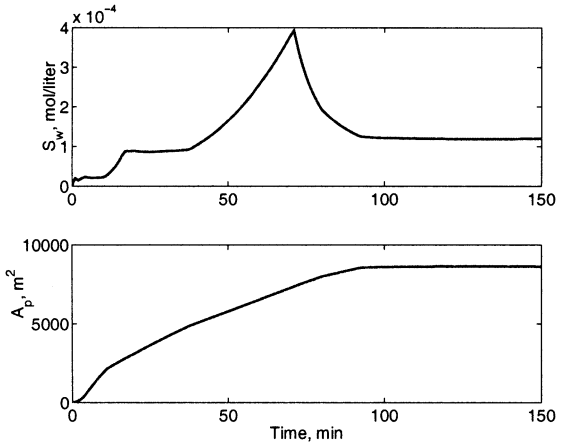

Figure 4. Free surfactant concentration S_w and the total swollen particle surface area A_p corresponding to the base case recipe.

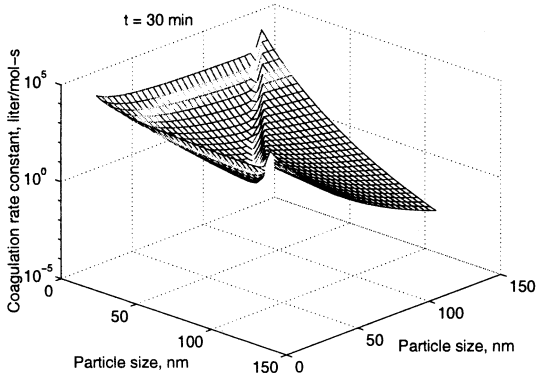

(a) $t = 30\ min$, $S_w = 0.9 \times 10^{-4}\ moles/liter$

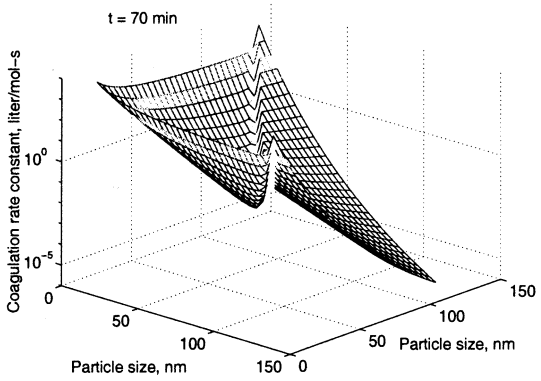

(b) $t = 70\ min$, $S_w = 3.8 \times 10^{-4}\ moles/liter$

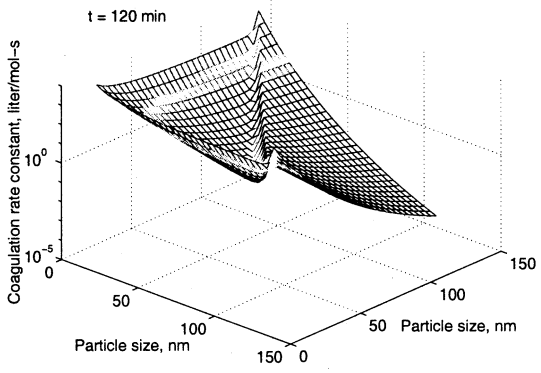

(c) $t = 120\ min$, $S_w = 1.2 \times 10^{-4}\ moles/liter$

Figure 5. Size-dependent intrinsic coagulation rate β—Eq. 14, reflecting the sensitivity of the repulsive potential to the free surface concentration S_w.

The rapid decrease in the coagulation rate constant at larger sizes can be exploited to reduce the computational load.

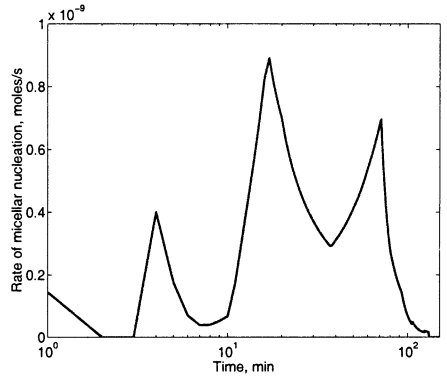

(a) micellar nucleation rate

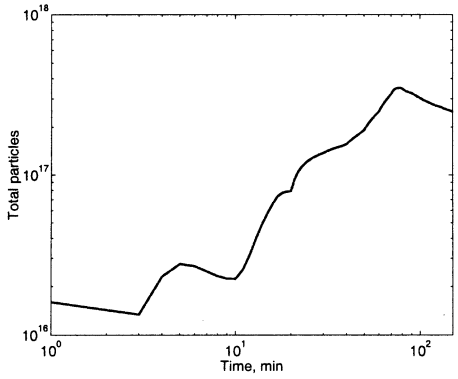

(b) profile of total particles

Figure 6. Profiles of the nucleation rate and total particles for the base case recipe.

at this time, compared to that at the other times. Figure 5 shows the intrinsic coagulation rates (coagulation kernel) corresponding to these same time instances, which reflect the sensitivity shown by the repulsive potential to the free surfactant concentration. The intrinsic coagulation rate is lower at 70 min relative to that at 30 min. Also, it is higher at 120 min by about four-fold compared to that at 70 min (not perceptible in the plot), as an effect of the variation in S_w. These results elucidate the potential to manipulate the coagulation rate by employing the surfactant feed.

Each of the plots in Figure 5 illustrate a rapid decrease in the coagulation rate constant with an increase in the particle size(s). This observation was exploited to further reduce the computational load. A cut-off size was fixed, above which the particles were assumed to be colloidally-stable, thereby eliminating the need to compute the coagulation terms for these larger size particles. This approach is consistent with earlier approaches. Richards et al. (1989) defined two particle populations, one accounting for the unstable smaller size particles, and the other for the stable larger size ones. A similar approach was adopted by Araujo et al. (2001) in a full population balance framework (resulting in two population balance equations). The present approach eliminates the need for two partial differential equations. However, a sensitivity study was performed to identify the suitable cut-off size.

The simulation results are analyzed further to study the evolution of the distribution. This analysis is also useful in the next subsection, in comparing the simulation results with the experimental data. Figures 6a and 6b show the rate of micellar nucleation and the profile of total particles over the

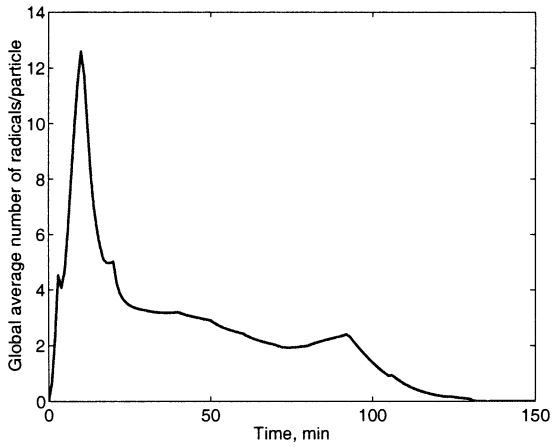

Figure 7. Global average number of radicals/particle, calculated from the complete distribution $\bar{n}(r,t)$, corresponding to the base case recipe.

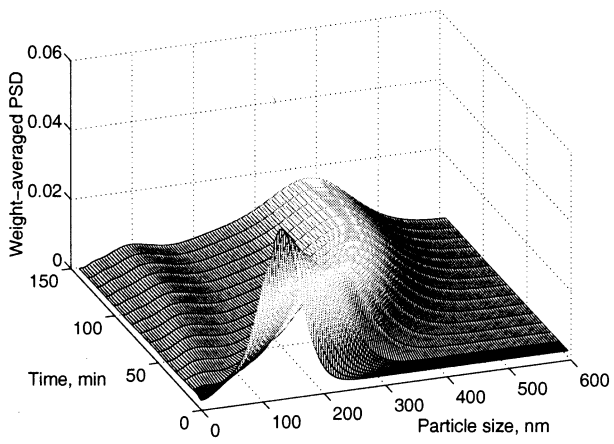

Figure 9. Evolution of the PSD along the course of the batch corresponding to the base case recipe.

course of the batch, respectively. The homogenous nucleation is restricted to very early times (before 1 min), contributing to the early particles seen in Figure 6b. On the contrary, micellar nucleation begins at about 1 min, and is prevalent through the entire course of the batch. The profile of the total particles records decreases in the particles count due to the coagulation events, which are seen to be the least evident at times of high free surfactant concentration (Figure 4). The high value of the intrinsic coagulation rate close to the end-point (Figure 5c), coupled with the higher particle concentration at these times, causes higher rates of coagulation towards the end of the batch, thereby leading to a large drop in the number of particles. Figure 7 shows the global average number of radicals/particle, $n_{ave}(t)$ calculated from the distribution $\bar{n}(r,t)$. It is seen that for most of the batch, $n_{ave}(t)$ is above unity justifying the use of a general model for a VAc-BuA copolymer system. Figure 8 shows the profile of the instantaneous overall conversion, which reaches about 78% at the end of 150 min with a modest solids content of about 22%. Figure 9 shows the evolution of the PSD along the course of the batch. The end-point PSD shows a large mode centered at approximately 400 nm, a diffuse mode at around 250 nm, and another mode at approximately 100 nm (separate plot shown later).

In summary, the model captures all relevant aspects of the evolution of the PSD, including the complications in the nucleation events associated with the nonionic surfactants (see Immanuel et al. (2002a, 2000) for such representative results). It can be employed to simulate all industrially-pertinent recipes, such as *ab initio* and seeded polymerizations.

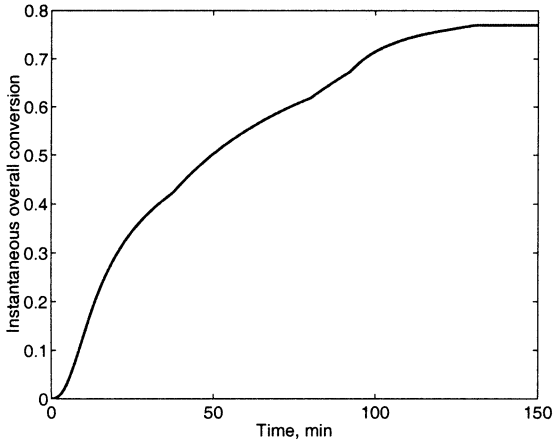

Figure 8. Instantaneous overall conversion of the monomers along the batch corresponding to the base case recipe.

Validation of the simulation results with experimental data

The comparison of the simulation results with the experimental data for various recipes is presented next. In the first comparison case, simulation results both with and without the coagulation events are presented to illustrate the improvement obtained in accounting for the coagulation phenomenon even under low solids conditions. The experimental facility comprises an on-line analyzer for PSD, the capillary hydro-dynamic fractionator (CHDF) from Matec Instruments, and an on-line densitometer. See Immanuel et al. (2002b) for more details on the facility and the experimental methods employed for the inference of process variables from the available measurements. Figure 10 compares the simulated end-point PSD and the profiles of the total particles and solids content (corresponding to the cases with and without coagulation), with the experimental data. The recipe for the experiment is the one shown in Figure 3 (base case), which was discussed in the previous subsection. The experimentally-observed distribution in Figure 10a (dashed line) shows diffuse and interconnected modes, one centered at approximately 320 nm, another at approximately 210 nm, and a third at approximately 70 nm. In the coagulation-free case (dash-dot line), the model simulates two diffuse and interconnected modes at the larger size end, similar to the experimental observation. However, it predicts a delayed, but larger, secondary micellar nucleation event (Figure 10b—dashed line), resulting in the separate and large peak centered at approximately 100 nm (Figure 10a). Parametric sensitivity

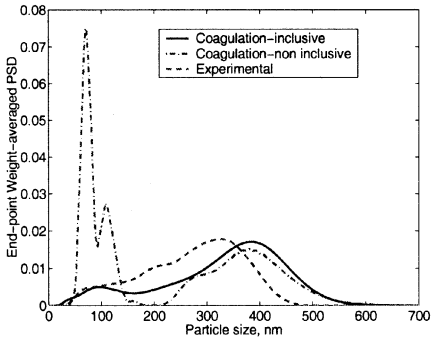

(a) comparison of the end-point PSD between the experimental and simulation results

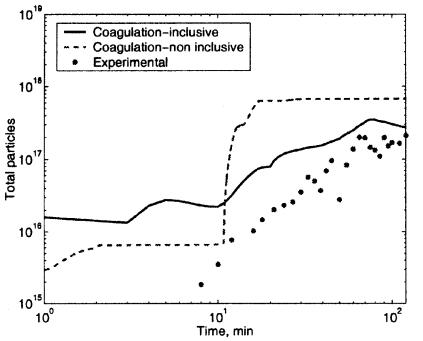

(b) comparison of the profiles of total particles

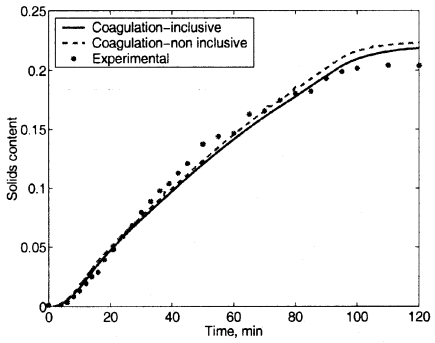

(c) comparison of the profiles of solids content, defined as (weight of polymer + surfactant)/(total weight of the latex)

Figure 10. Simulation results vs. experimental data for the vinyl acetate-butyl acrylate copolymerization recipe shown in Figure 3 (base case).

study indicates that this discrepancy is not entirely due to the uncertainty in the values of the parameters (Immanuel et al., 2002a, 2001). On the other hand, the coagulation-inclusive simulation result captures these interconnected nucleation events well, and also preserves the relative magnitudes of the various peaks, as seen in Figures 10a and 10b. However, in the simulation results, the early modes are still larger than in the experimental data. Such discrepancies seen in the profiles and the distribution can be attributed to the parametric uncertainty. Thus, there are clear improvements obtained upon incorporating coagulation events into the model, the complete model showing a qualitative and a partly quantitative validity.

A detailed parametric sensitivity study was performed with the coagulation-inclusive model. Based on this study, some of the parameters were adjusted (c_1, c_2, Γ_∞, K_{ad}, cmc, k_{r1} and k_{t11}) to best match the simulated PSD with the experimentally-observed PSD (Table 1). The matching of the experimental and simulated profiles (total particles, solids content) was not considered in this parameter identification exercise. However, there are several sources of uncertainty in the experimental results, caused by discrepancies in the feed rates delivered by the pumps, delays in step changes in the feed rates, temperature fluctuations and so on, which need to be accounted for in a more rigorous parameter identification exercise. The parameter values determined here are employed for all subsequent simulations without further adjustment. Also, the complete coagulation-inclusive results alone are presented henceforth, to make the plots more legible.

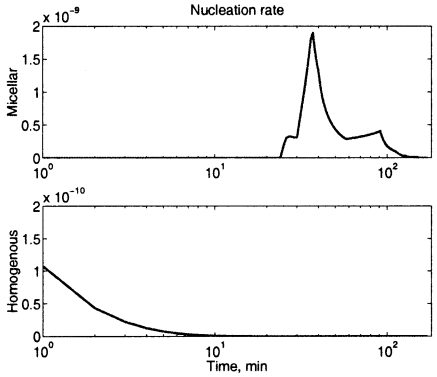

(a) micellar and homogenous nucleation rates in units of moles/s along the course of the batch

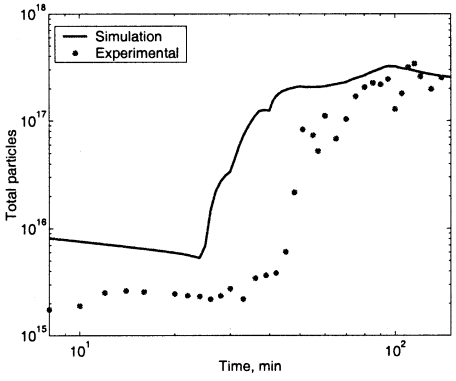

(b) comparison of the profile of total particles along the course of the batch

Figure 11. Nucleation rates and total particles profile for a recipe in which the feed of the monomers and the surfactant solution shown in Figure 3 is delayed by 20 min (the initial mixture contains VAc monomer, but no surfactant).

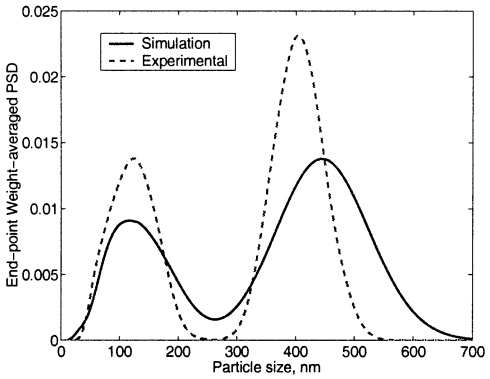

(a) comparison of the end-point PSD between the experimental and modeling results

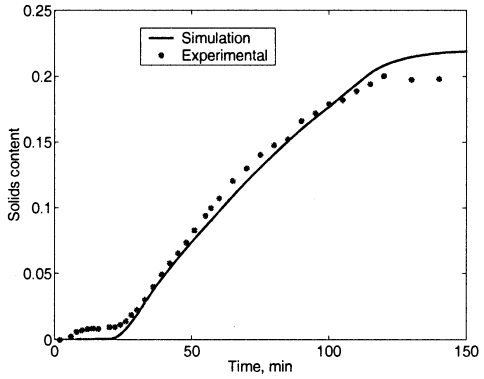

(b) comparison of the profile of solids content

Figure 12. Simulation vs. experimental results for a recipe with delayed feed of surfactant and monomer (corresponding to the case in Figure 11).

Figure 11 shows the simulation results pertaining to a different recipe, and Figure 12 compares the predictions of the end-point PSD and the profile of solids content with the corresponding experimental data. In this case, while the initial mixture was the same as in the base case, the feed of VAc, BuA, and surfactant solution was delayed by 20 min. During the first 20 min of the batch, no external surfactant or BuA monomer was present in the reactor. When the initiator components tBHP and SFS (which are not delayed) enter the reactor, the VAc monomer in the initial batch (52 g) is initiated, and particles are formed by the homogenous mechanism (Figure 11a—lower plot). Homogenous nucleation rate remains appreciable until about 10 min, because of the higher solubility of the VAc monomer in the aqueous phase. Thereafter, there is a decline in the number of particles (Figure 11b) due to coagulation. At about 20 min, the feed of surfactant and the two monomers is started. Micellar nucleation begins shortly after this, and is prevalent for most part of the batch (Figure 11a). The resultant PSD at the end of the batch is a prominent bimodal distribution, shown in Figure 12a (solid line). The comparison of the experimental data on the end-point distribution (Figure 12a) and the profiles of total

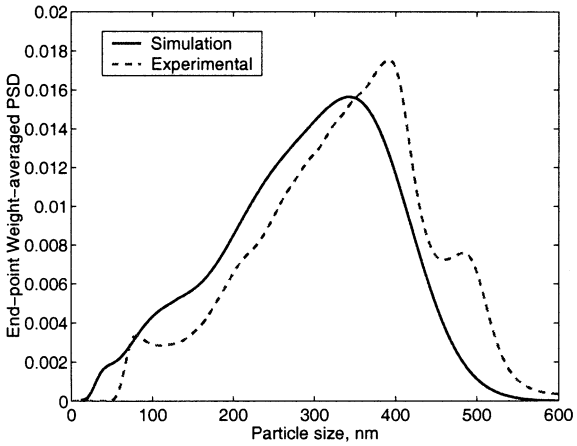

Figure 13. Simulation vs. experimental end-point PSD for a recipe obtained by a 22% reduction in the BuA feed rate relative to Figure 3, up to 94 min.

particles (Figure 11b) and solids content (Figure 12b), with the corresponding simulation results, shows a reasonable match. (Note that the plot in Figure 12a is of the relative distribution, which causes the simulated peaks to be lower due to the presence of particles bridging the two modes.)

Figures 13–16 compare the simulations and experiments for four different recipes, which were obtained by perturbations in the feed rates of BuA, VAc, surfactant solution and initiator solution, respectively, with respect to the recipe shown in Figure 3. In each case, the simulation results show very similar qualitative trends with the experimental results, in terms of the nucleation, growth, and coagulation events. These are evident by a comparison of the number of modes and their relative magnitudes between the simulations and the experimental data. The simulation results corresponding to the base case (particularly Figure 6a) are used as a reference to interpret these results.

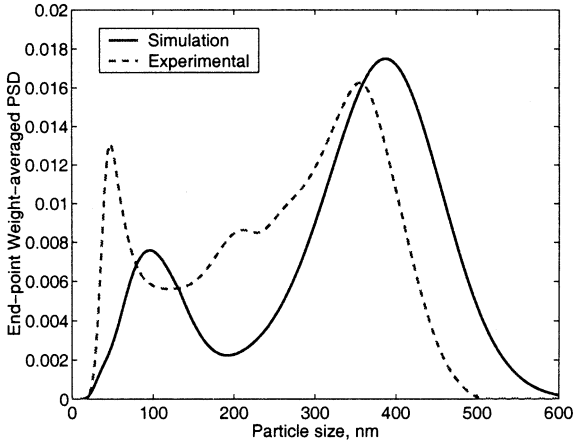

Figure 14. Simulation vs. experimental end-point PSD for a recipe obtained by a 28% reduction in the VAc feed shown in Figure 3 up to 16.7 min.

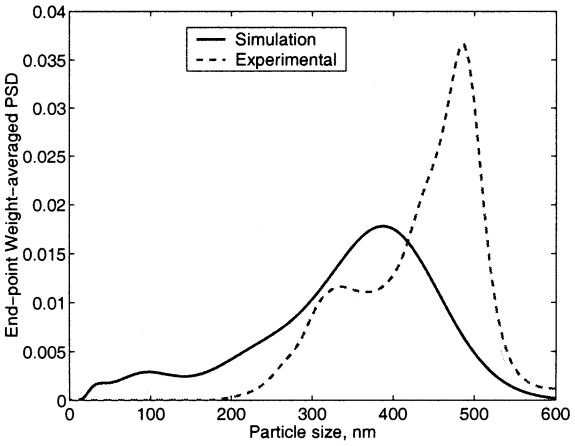

Figure 15. Simulation vs. experimental end-point PSD for a recipe in which the step increase in the surfactant feed at 10 min, shown in Figure 3, is delayed to 15 min.

Figure 13 corresponds to a recipe in which the BuA feed rate was reduced by 22% relative to the original recipe (base case) up to 94 min, and, thereafter, the feed rate was raised to the level in Figure 3. The total quantity of BuA in the recipe was maintained the same as in the earlier recipe. The VAc-BuA co-polymerization system is characterized by a high reactivity ratio, with BuA being the more reactive monomer. For this reason, the reduced BuA feed results in much reduced growth rates (relative to the base case), and, hence, a high free surfactant concentration and micellar nucleation rate between 3–6 min (see Figure 6a). This in turn cascades into a reduced micellar nucleation rate at the later times. After 94 min, there is a substantial increase in the reaction rates, that results in the de-swelling of the particles (due to the monomer consumption) and the release of the surfactants (*adsorbed* onto their surface) back into the aqueous phase. This in turn causes enhanced nucleation rates towards

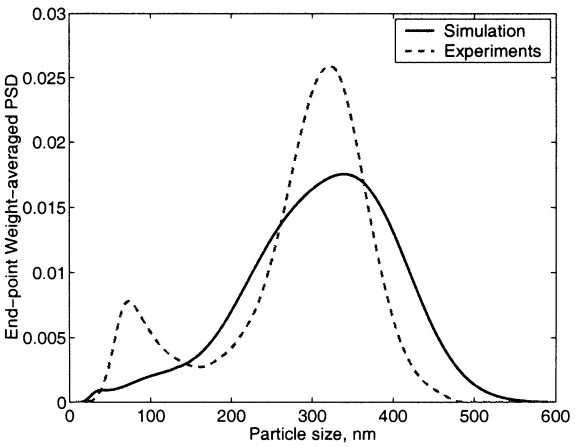

Figure 16. Simulation vs. experimental end-point PSD for a recipe in which the concentration of initiator components is doubled compared to the recipe shown in Figure 3.

the end of the batch. Hence, the broad PSD seen in Figure 13. Also, both the simulation and the experimental PSD show the same trend.

For the result presented in Figure 14, the VAc feed rate up to 16.7 min was reduced by 28% compared to Figure 3. There was a prolonged feed of VAc due to this, in order to maintain the same amount of VAc in the two recipes. In the perturbed case, there is a larger value of the average number of radicals/particle at early times, and, hence, larger growth rates. This results in reduced nucleation rates between 3–6 min (Figure 6a). The monomer droplets disappear from the system earlier in this case (before 12 min), resulting in the release of surfactants *absorbed* into them back into the aqueous phase. This causes a more prominent nucleation at these times. Both the simulation and the experimental results show the same trend, although the simulation predicts an even smaller nucleation at the intermediate times (3–6 min)—attributable to uncertainty in the surfactant partitioning parameters.

In the case of Figure 15, the step increase in the surfactant feed rate at 10 min in Figure 3 was delayed to 15 min. The monomer droplets disappear in both cases at about 12 min, releasing the *absorbed* surfactants into the aqueous phase, and thereby resulting in increased rates of micellar nucleation (again, see Figure 6a). However, in the current case, there is a relatively reduced micellar nucleation at this time, but a more substantial nucleation event at later times. Although the experimental result shows a larger growth rate, and/or an earlier completion of the nucleation events compared to the simulation results, the overall trend is very similar (with the simulated PSD being a stretched version of the experimental one).

Figure 16 presents results in which case the concentration of the initiator components were doubled relative to that employed in the base case recipe. In the current case, there is a larger homogenous nucleation initially, which results in lower values of $\bar{n}(r,t)$, and, hence, lower growth rates. This causes the total surface area to be lower, thereby raising the value of S_w and the nucleation rates in the 3–6 min time range. Soon after, the value of $\bar{n}(r,t)$ increases, causing the surface area A_p to increase above that in the base case (higher concentration of the initiator components), and in turn causing reduced rates of nucleation. This results in the PSD seen in the figure. The larger mode comprises the particles nucleated up to about 6 min (initial homogenous and the intermediate micellar nucleation events). The tail corresponds to the particles nucleated at later times of the batch. The experimental results show a more prominent secondary peak. This could be either due to an even earlier (and, hence, reduced) primary micellar nucleation event before 3 min in the experimental case, or due to the later nucleation events occurring at larger rates than predicted.

Figure 17 considers a different family of recipe for a batch spanning 200 min. In this case, the solids content achieved is slightly higher than the other cases, under which condition one can expect more coagulation events. The experimental results show three peaks, at approximately 70 nm, 320 nm, and 500 nm, and a shoulder at about 200 nm. The simulated distribution also shows these modes, although the corresponding peak sizes are staggered. Also, there is an overall preservation of the relative magnitudes of the various peaks.

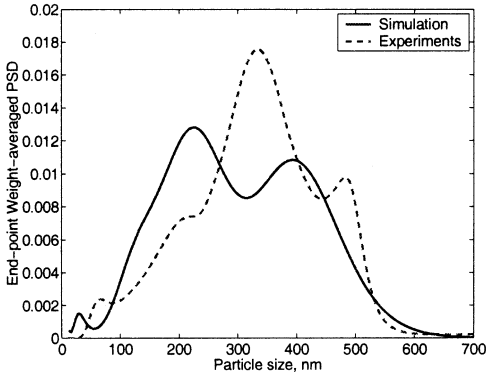

(a) comparison of the end-point particle density function between the experimental and modeling results

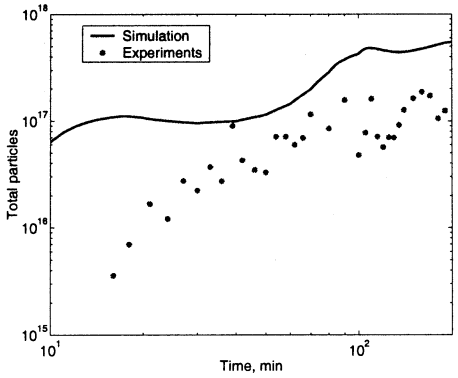

(b) comparison of the total particles

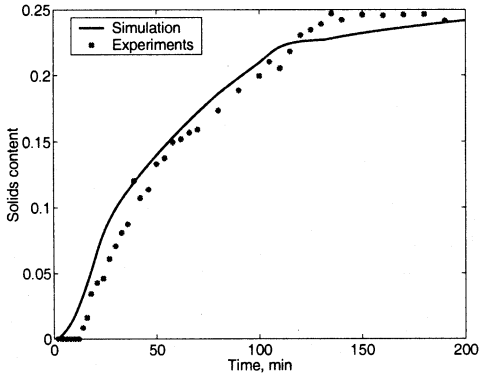

(c) comparison of the solids content

Figure 17. Simulation vs. experimental results for a different family of recipe, aimed at achieving a higher solids content, and involving a longer batch time.

Summary

A population balance model is developed for the PSD in emulsion polymerization, accounting for the nucleation, growth, and coagulation phenomena. The system under consideration is the co-polymerization of vinyl acetate (VAc) and butyl acrylate (BuA) with nonionic surfactants and redox initiators. In addition to consolidating the various theories on each of these phenomena into a single study, the model presented here and in a prequel (Immanuel et al., 2002a) proposes several modifications to the population balance model for PSD in emulsion polymerization. A significant modification as regards to the nucleation event is the incorporation of the partitioning of the surfactants into the bulk of the dispersed phases, which accounts for the alterations in the nucleation pattern under nonionic surfactants. In modeling the growth phenomenon, a first principles-based formulation is proposed to model the average number of radicals/particle. The proposed formulation preserves the size-dependence of the growth kernel, captures the broadening of the distributions with growth (both effects seen experimentally), and also obviates the need for incorporating artificial dispersion terms in the population balance equation. The improvements obtained with this modification clearly indicate the disadvantages with lumped parameter modeling, and motivate the use of a distributed approach where possible. The major contribution of this article is on the coagulation mechanism. The calculation of the size-dependent intrinsic coagulation rate and the coagulation terms for emulsion recipes employing nonionic surfactants is demonstrated. Steric stabilization under the influence of *adsorbed* surfactants is modeled as the primary stabilizing mechanism. However, empirical allowances are introduced into the calculations to account for other mechanisms that influence coagulation, including the shear imparted on the particles due to the mixing in the reactor. In formulating the population balance equation, the particle size is used as the internal coordinate. This is mainly due to two reasons, namely that the measurement available is as a size distribution (and not volume distribution, for example), and that the range of particle size is narrower than the range of particle volume, which makes the choice of size beneficial with respect to a numerical solution (number of finite elements, and so on). This choice of size as the internal coordinate introduces minor, although critical, changes to the coagulation kernel, which are clearly developed in this article.

The model can be used to simulate all types of emulsion recipes that are of interest to practitioners. The simulation results were compared with experimental data. In general, the model demonstrates a good ability to predict the experimental observations. Also, there is a substantial improvement over the previous coagulation-free simulation results. The discrepancies between the complete coagulation-inclusive simulation results and the experimental observations can be attributed not only to parametric uncertainty, but also experimental uncertainty (disturbances, delays in pump startups, errors in the feed rates, and so on). The cascaded effects of the parametric uncertainties on the evolution of the distribution were also discussed. The parameters were adjusted manually to provide an overall fit of the end-point PSD in one case, and the same set of parameters were used in the simulation of all the cases. It might be beneficial to perform a rigorous (parameter) identification, utilizing all the experimental cases, and simultaneously accounting for experimental uncertainties. In such an exercise, it would be appropriate to consider matching the profiles of total particles and solids content (rather than matching the end-point distribution).

This objective has the advantage that it in effect matches the entire trajectory of the distribution, and has been shown to be advantageous for the control of PSD (Immanuel and Doyle III, 2002d). For the purposes of on-line control of PSD, a combined parameter-state estimator can be employed to account for the uncertainties in the model simultaneously, while inferring the relevant feedback informations necessary for control (Immanuel and Doyle III, 2002a).

Acknowledgments

The authors acknowledge the help of Professor Eric W. Kaler at the University of Delaware on the coagulation modeling concepts, and financial support from the University of Delaware Competitive Fellowship for C. D. Immanuel and from the Office of Naval Research and the University of Delaware Process Control and Monitoring Consortium.

Notation

A = Hamakar constant
A_p^s = total swollen surface area of particles
cmc = critical micelle concentration
D_0 = effective diffusion coefficient
$F(r,t)$ = particle density function
$F_R(D)$ = repulsive force between particles separated by distance D
j_{cr} = critical chain length
k = Boltzmann constant
k_{ri} = rate constant for reaction between initiator and monomer i
k_{tij} = rate constant for termination of polymer of type i with another polymer of type j
K_{ad} and Γ_∞ = Langmuir adsorption constants
l = effective length of a segment of surfactant chain
L = extension length of adsorbed surfactant into the aqueous phase
$n_{ave}(t)$ = global average number of radicals per particle
$\bar{n}(r,t)$ = average number of active radicals in particles of size r at time t
N_A = Avogadro number
r = particle radius
$r_{cut\text{-}off}$ = size above which the particles are colloidally-stable
$r_{micelle}, r_{nuc}$ = radius of a micelle/nucleation size
R_F = Flory radius
R_g = radius of gyration
sc = solids content of latex
sc_{ref} = reference solids content
S_w = free surfactant concentration
T = reactor temperature
$W(r,r')$ = Fuch's stability ratio for particles of size r and r'
α = interaction parameter between polymer (surfactant) and solvent (water)
$\beta(r,r')$ = intrinsic coagulation rate between particles of size r and r'
μ = viscosity of latex
μ_0 = viscosity of water
$\psi_R^f(D)$ = repulsive potential between flat objects separated by distance D
$\psi_R(D)$ = repulsive potential between spherical particles separated by distance D

Literature Cited

Araujo, P. H. H., J. C. de la Cal, J. M. Asua, and J. C. Pinto, "Modeling Particle Size Distribution (PSD) in Emulsion Copolymerization Reactions in a Continuous Loop Reactor," *Macromol. Theory Simul.*, **10**, 769 (2001).

Chen, S., and K. Wu, "Emulsion Polymerization: Theory of Particle Size Distribution in Copolymerization Systems," *J. of Poly. Sci., Part A: Poly. Chemistry Ed.*, **26**, 1487 (1988).

Coen, E. M., R. G. Gilbert, B. R. Morrison, H. Leube, and S. Peach, "Modeling Particle Size Distributions and Secondary Particle Formation in Emulsion Polymerisation," *Polymer*, **39**, 7099 (1998).

Crowley, T. J., E. S. Meadows, E. Kostoulas, and F. J. Doyle III, "Control of Particle Size Distribution Described by a Population Balance Model of Semibatch Emulsion Polymerization," *J. Proc. Cont.*, **10**, 419 (2000).

Evans, D. F., and H. Wennerstrom, *THE COLLOIDAL DOMAIN Where Physics, Chemistry, Biology, and Technology Meet*, 2nd ed., Wiley-VCH, New York (1999).

Fritz, G., V. Schadler, N. Willenbacher, and N. J. Wagner, "Electrosteric Stabilization of Colloidal Dispersions," *Langmuir*, in press (2002).

Gilmore, C. M., G. W. Poehlein, and F. J. Schork, "Modeling Poly (Vinyl Alcohol)-Stabilized Vinyl Acetate Emulsion Polymerization: I. Theory," *J. Appl. Polym. Sci.*, **48**, 1449 (1993).

Immanuel, C. D., and F. J. Doyle III, "A Hierarchical Strategy for Control of Particle Size Distribution Using Multi-Objective Optimization," *AIChE J.*, (2002a).

Immanuel, C. D., and F. J. Doyle III, "Computationally-Efficient Solution of Population Balance Models Incorporating Nucleation, Growth and Coagulation," *Chem. Eng. Sci.*, submitted (2002b).

Immanuel, C. D., and F. J. Doyle III, "Open-loop Control of Particle Size Distribution in Semi-batch Emulsion Co-Polymerization using a Genetic Algorithm," *Chem. Eng. Sci.*, **57**, 4415 (2002c).

Immanuel, C. D., and F. J. Doyle III, "Tracking of a Reference Particle Size Distribution Trajectory in Semibatch Emulsion Polymerization," *Proc. Amer. Control Conf.*, Anchorage, AK, Omnipress, Madison, WI, 1007 (2002d).

Immanuel, C. D., C. F. Cordeiro, S. S. Sundaram, E. S. Meadows, T. J. Crowley, and F. J. Doyle III, "Modeling of Particle Size Distribution in Emulsion Co-Polymerization: Comparison with Experimental Data and Parametric Sensitivity Studies," *Comp. Chem. Eng.*, **26**, 1133 (2002a).

Immanuel, C. D., F. J. Doyle III, and C. F. Cordeiro, "Parametric Sensitivity and Model Validation for Particle Size Distribution in Emulsion Polymerization," *Proc. Int. Wkshp. on Pol. Rea. Eng., DECHEMA Monograph*, Vol. 137, Hamburg, Germany, Wiley-VCH, Weinhein, Germany, 313 (2001).

Immanuel, C. D., T. J. Crowley, E. S. Meadows, and F. J. Doyle III, "Fundamental Modeling of Particle Size Distribution in Emulsion Co-polymerization," AIChE Meeting, Los Angeles (2000).

Immanuel, C. D., T. J. Crowley, E. S. Meadows, C. F. Cordeiro, and F. J. Doyle III, "An Experimental Study of the Evolution of Multi-Modal Particle Size Distribution in Vinyl Acetate-Butyl Acrylate Emulsion Co-Polymerization," *J. Polym. Sci., Polym. Chem.*, in press (2002b).

Israelachvili, J., *Intermolecular and Surface Forces*, 2nd ed., Academic Press (1998).

Kiparissides, C., I. Moustakis, and A. Hamielec, "Electrostatic and Steric Stabilization of PVC Primary Particles," *J. Appl. Polym. Sci.*, **49**, 445 (1993).

Meadows, E. S., T. J. Crowley, C. D. Immanuel, and F. J. Doyle III, "Non-isothermal Modeling and Sensitivity Studies for Batch and Semi-batch Emulsion Polymerization of Styrene," *Ind. Eng. Chem. Res.*, **42**, 555 (2003).

Melis, S., M. Kemmere, J. Meuldijk, G. Storti, and M. Morbidelli, "A Model for the Coagulation of Polyvinyl Acetate Particles in Emulsion," *Chem. Eng. Sci.*, **55**, 3101 (2000).

Min, K. W., and W. H. Ray, "On the Mathematical Modelling of Emulsion Polymerization Reactors," *J.M.S.-Rev. Macromol. Chem.*, **C11**, 177 (1974).

Napper, D. H., *Polymeric Stabilization of Colloidal Dispersions*, Academic Press, London (1983).

Ozdeger, E., E. D. Sudol, M. S. El-Aasser, and A. Klein, "Role of Nonionic Surfactant Triton X-405 in Emulsion Polymerization. III. Copolymerization of Styrene and n-Butyl Acrylate," *J. of Poly. Sci.: Part A: Poly. Chem.*, **35**, 3837 (1997).

Piirma, I., and M. Chang, "Emulsion Polymerization of Styrene: Nucleation Studies with Nonionic Emulsifier," *J. of Poly. Sci.: Poly. Chem. Ed.*, **20**, 489 (1982).

Rawlings, J. B., and W. H. Ray, "The Modeling of Batch and Continuous Emulsion Polymerization Reactors. Part I: Model Formulation and Sensitivity to Parameters," *Poly. Eng. Sci.*, **28**, 237 (1988a).

Rawlings, J. B., and W. H. Ray, "The Modeling of Batch and Continuous Emulsion Polymerization Reactors. Part II: Comparison with Experimental Data from Continuous Stirred Tank Reactors," *Poly. Eng. Sci.*, **28**, 257 (1988b).

Richards, J. R., J. P. Congalidis, and R. G. Gilbert, "Mathematical Modeling of Emulsion Copolymerization Reactors," *J. of Appl. Poly. Sci.*, **37**, 2727 (1989).

Saldivar, E., P. Dafniotis, and W. H. Ray, "Mathematical Modeling of Emulsion Copolymerization Reactors: I. Model Formulation and Application to Reactors Operating with Micellar Nucleation," *J.M.S.-Rev. Macromol. Chem. Phys.*, **C38**(2), 207 (1998).

Manuscript received Oct. 2, 2002, and revision received Jan. 16, 2003.